Adaptive Backstepping Sliding Mode Control for Speed of PMSM and DC-Link Voltage in Bidirectional Quasi Z-Source Inverter

Cong-Thanh Pham(✉), Chan Thanh Nguyen Huu, Quoc-Khai Tran, Tran Van Thien, and Duc Tam-Hong Nguyen

Faculty of Electrical and Electronic, Vietnam Aviation Academy, Ho Chi Minh City 700000, Vietnam
{thanhpc,thanhnhc,khaitq,thientv,ducnth}@vaa.edu.vn

Abstract. Researching and designing the controller for speed of permanent magnet synchronous motor (PMSM) and the DC-link voltage controller (DCV) in bidirectional quasi z-source inverter (BQ-ZSI) have a strong influence on the efficiency of electric vehicle applications. This paper presents two control strategies: Firstly, the speed of PMSM is controlled via sliding mode control (SMC) and adaptive backstepping which are called SA; Secondly, the peak of DCV in BQ-ZSI is regulated by controlling the total of the two capacitor voltages of BQ-ZSI. When the system operates, limitations of inverter current and voltage level on the motor output power have been reduced. With these strategies, DCV and speed of PMSM are stabilized, which improve the system efficiency. To demonstrate the effectiveness of the proposed method, the PMSM drive model and the controllers are simulated using MATLAB software.

Keywords: Z-source inverter · PMSM · Quasi-Z-source inverter · Backstepping Control · Sliding Mode Control

1 Introduction

Permanent magnet synchronous motor (PMSM) is a type of AC motor commonly used in industrial rotating systems, especially in the electric vehicles (EVs) [1]. Research on controller design with the aim of reducing errors, reduces costs and improving performance is increasingly interested by many researchers [2–5]. In recent years, the main method for controlling the speed of the PMSM is the field oriented control (FOC) scheme, where one speed and two current loops are decoupled on dq-axis [6]. The speed controller of motor is designed to track reference speed and it also generates a reference current signal on q-axis, two current controllers are used to stabilize the voltage on d and q-axis [7].

In PMSM drive systems, the speed controller is designed to satisfy the requirements of the control systems such as: a wide adjustable speed range, adaptation to high instantaneous torque response, load disturbances and parameter

N.-S. Vo and H.-A. Tran (Eds.): INISCOM 2023, LNICST 531, pp. 185–202, 2023.
https://doi.org/10.1007/978-3-031-47359-3_14

variations, low error ripple speed, low ripple torque, reliability, high efficiency and robustness. Therefore, the fixed coefficients K_p, K_i and K_d of traditional PID controller are not inconsonant with the high performance requirements of systems. Many artificial intelligence techniques were used to adjust the gains of the PID controllers as: genetic algorithms (GA) and particle swarm optimization (PSO) [8]. However, in order to achieve online gain tuning of the PI controllers, the speed of the microcontroller and the convergence speed of the GA and PSO must be fast, leading to a high computational burden [9]. Therefore, the study of an adaptive back-stepping controller is applied for controlling the speed motor which it is given in this paper.

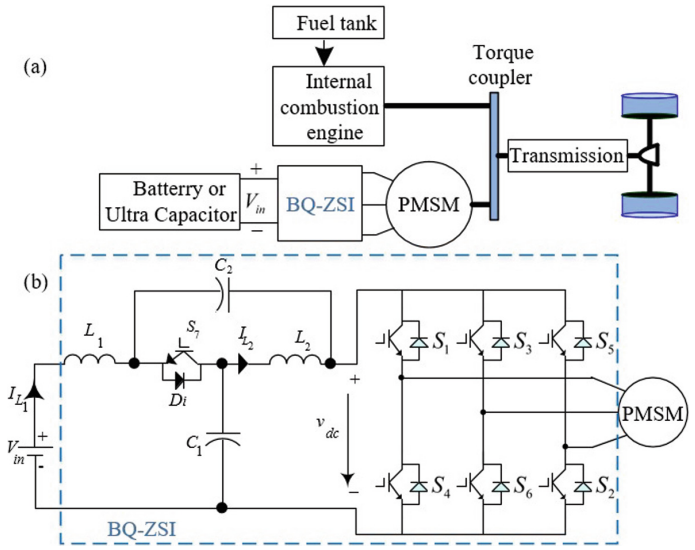

Fig. 1. The bidirectional quasi-Z-source inverter topology.

When applying the PMSM for electric vehicles, voltage source inverters with direct current (DC) voltage are used as battery. At high current, when the battery discharges, the voltage of battery decreases greatly and when the battery charges the voltage of battery increases greatly [10]. The voltage drop will impact the output power, speed motor, load torque and performance of PMSM drives system. The bidirectional DC to DC converter topology is applied to convert energy back and forth in the system between DC source supply and inverter. It can correct the mismatch between the DC power source and the DC-link voltage (DCV) of inverter and also ensures that the DCV is always kept stable.

In 2003, F.Z.Peng proposed Z-source inverter (ZSI) which is a boost/buck converter, it solves many of the disadvantages of traditional voltage source converters. [11]. The DCV is adjusted by changing duty in ZSI so that it increases the reliability of ZSI. Comparing with ZSI, QZSI has the advantages as low stress

on the voltage and continuous current, the power transfers on directional flow from the DC source to the AC side [12]. The bidirectional quasi-Z-source inverter (BQ-ZSI) as response requirements of EV that is able to reverse the direction of power transmission when the motor is decelerating or braking, the energy from PMSM can be transferred back to the source with an additional seventh switch. The current of the inductor is always continuous and small inductance in BQ-ZSI topology have a better effective which it is suitable for electric vehicle applications as Fig. 1 on page 2 a) and b).

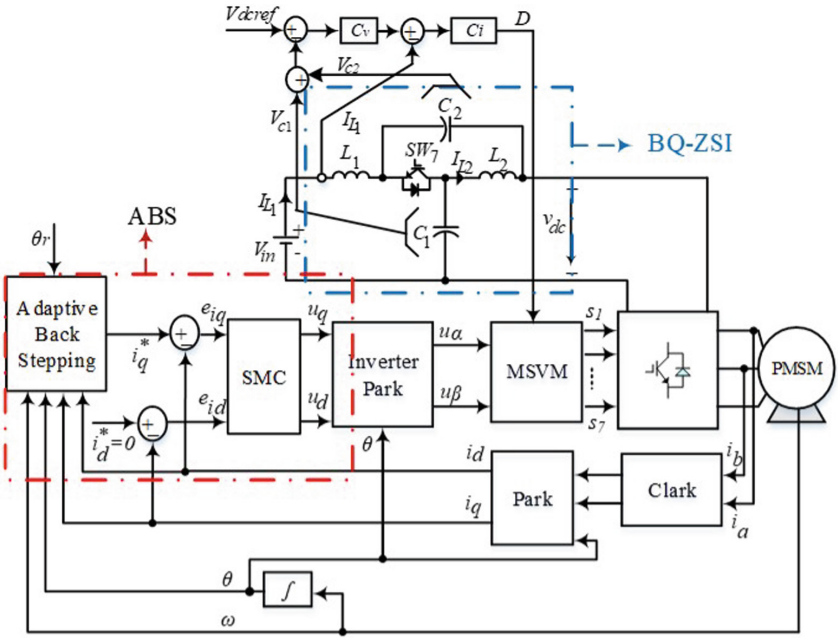

Fig. 2. The adaptive Backstepping Speed Control in PMSM Fed by a BQ-ZSI topology.

This paper studies the application of BQ-ZSI scheme for the PMSM drive for electric vehicle. Moreover, two control algorithms between the DC source and the AC side of the PMSM drive for electric vehicle are presented: the first one is the speed control motor (AC side controller) based on adaptive backstepping and sliding mode control; the second one is to control the peak DCV in BQ-ZSI (DC side controller) based on the regulation of the two capacitors voltages when the input DC voltage (battery or super capacitor) of BQ-ZSI is dropped durring EV operation (the load torque and the speed of the motor change continuously). As a result, the efficiency of the electric vehicle system is enhanced.

The organization of this paper include as: Sect. 2 introduces the description of PMSM drive system and the BQ-ZSI scheme. Section 3 presents the two proposed controllers for the speed motor and the BQ-ZSI. Section 4 discusses the

simulation results on MATLAB software and Sect. 5 concludes the effectiveness of the proposed methods.

2 Description PMSM and BQ-ZSI Scheme

2.1 Description PMSM Drive System

The mathematical model of the PMSM drive system is derived in the $d-q$ axis as:

$$\begin{cases} \dot{\omega} = -\frac{B}{J}.\omega - \frac{T_L}{J} + \frac{1.5 n_p \Psi_f}{J} i_q \\ \dot{i}_d = \frac{R_s}{L_d} i_d + n_p \omega i_q + \frac{1}{L_d} u_d \\ \dot{i}_q = -n_p \omega i_d - \frac{R_s}{L_d} i_q - n_p \frac{\Psi_f}{L_q} \omega + \frac{1}{L_q} u_q \\ \dot{\theta} = \omega \end{cases} \tag{1}$$

In which ω is the rotor speed. u_d, u_q,i_d, i_q are the voltages and stator currents, respectively, in the dq-axes frame. The limited voltage is λ on dq-axis, which $|u_d| \leq \lambda$ and $|u_q| \leq \lambda, (\lambda < 1)$. The stator inductance are L_d, L_q and without any loss of generality, the asumption $L_d = L_q$ is valid [6]. Ψ_f, R_s, J, T_L, B, and n_p are respectively the permanent magnet flux linkage, the stator resistance, the moment of inertia, the load torque, the viscous friction coefficient, and the number of pole pairs.

2.2 Analysis of the BQ-ZSI Network Modeling

The structure diagram of the BQ-ZSI is presented in Fig. 1 which is called DC-side model. There are two operating as belows: 1) the bidirectional quasi z-source network (BQ-ZSN), which is comprised of C_1, C_2, L_1, L_2, and switch $S_7$with a parallel diode D_i. 2) the three-phase inverter. With these two switches, the power flow can be controlled bidirectionally. The three-phase bridge include six switch and the motor is replaced by R_l and L_l.

The BQ-ZSI has three common operating states: the non shoot-through state (NST), the zero state, and the shoot-through state (ST) [13]. In the ST, the DCV (V_{dc}) is boosted by conducting the lower and upper switches of the three-phase inverter at the same time.

From Fig. 1b), it also shows that the BQ-ZSI allows the inductor current to flow continuously in both two directions. When the three-phase inverter is in the ST with S_i close circuit as Fig. 3a), the diode D_i is reversely blocked, the switch S_7 is open circuit, the current and the voltage on capacitors and inductors are shown as Fig. 3a). When the three-phase inverter is in the NST as Fig. 3b), the switch S_7 is close circuit and the power back to the DC source input through switch S_7, this is in the generatoring mode of BQ-ZSI. Instead, the power through diode transfer inverter [12]. Therefore, at all operating conditions, the continuous conduction mode of the BQ-ZSI is maintained and the performance of the three phases inverter is enhanced. This property is very good for EV applications.

The state variables $x(t)$ of this BQ-ZSI model are shown as Fig. 3. The inductor currents through L_1, L_2as $(i_{L_1}(t))$ and $(i_{L_2}(t))$. The capacitor voltages C_1, C_2 are $v_{C_1}(t)$ and $v_{C_2}(t)$. The load current is $i_{lo}(t)$. The variables is $c(t)$, $c(t) = v_{in}(t)$.

$$\text{Set } x(t) = \begin{bmatrix} i_{L_1}(t) \\ i_{L_2}(t) \\ v_{C_1}(t) \\ v_{C_2}(t) \\ i_{lo}(t) \end{bmatrix}$$

– In the ST, the switch S_7 and diode D_i are closed circut, S_i is close circuit, the circuit as Fig. 3a). In the state space form, the equation group can be written: $A.\dot{x}(t) = B_1.x(t) + C_1.c(t)$, where

$$A = \begin{bmatrix} L_1 & 0 & 0 & 0 & 0 \\ 0 & L_2 & 0 & 0 & 0 \\ 0 & 0 & C_1 & 0 & 0 \\ 0 & 0 & 0 & C_2 & 0 \\ 0 & 0 & 0 & 0 & L_l \end{bmatrix}; B_1 = \begin{bmatrix} 0 & 0 & 0 & 1 & 0 \\ 0 & 0 & 1 & 0 & 0 \\ 0 & -1 & 0 & 0 & 0 \\ -1 & 0 & 0 & 0 & 0 \\ 0 & 0 & 0 & 0 & -R_l \end{bmatrix}; C_1 = \begin{bmatrix} 1 \\ 0 \\ 0 \\ 0 \\ 0 \end{bmatrix}$$

– In the NST, the switch S_7 and diode D_i are close circuit, the switch uper and lo S_i is open circuit, the circuit as Fig. 3b). Similar, in the state space form, the equation group can be obtained as $A.\dot{x}(t) = B_2.x(t) + C_2.c(t)$, where

$$B_2 = \begin{bmatrix} 0 & 0 & -1 & 0 & 0 \\ 0 & 0 & 0 & -1 & 0 \\ 1 & 0 & 0 & 0 & -1 \\ 0 & 1 & 0 & 0 & -1 \\ 0 & 0 & 1 & 1 & -R_l \end{bmatrix}; C_2 = \begin{bmatrix} 1 \\ 0 \\ 0 \\ 0 \\ 0 \end{bmatrix}$$

Where the D_u is shoot-through duty. The D'_u is non shoot-through duty, in one of switching period (T_{sf}). Total duty is calculated in one of switching period as: $D_u + D'_u = 1$.

With the switching period T_{sf} of the space vector modulation, the BQ-ZSI state-average of each state matrix is processed as below:

$$A\dot{\bar{x}} = [D_u B_1 + (1 - D_u) B_2] \bar{x} + [D_u C_1 + (1 - D_u) C_2] \bar{c} \tag{2}$$

In which $\bar{x}$ and X are state variable period average and balance operation point. Farther, in the operation points, state variable has a small signal disturbances with low frequency which are presented as: $\bar{x} = X + \hat{x}$; $\bar{d}'_u = 1 - \bar{d}_u$; $\bar{c} = C + \hat{c}$; $\bar{d}_u = D_u + \hat{d}_u$;

In space vector modulation method, the switching frequency of S_i in three-phases inverter is fast. Hence, around the operation points of the BQ-ZSI system which is linearized and the steady-state of this system has Eq. (2) as belows:

$$0 = [D_u.B_1 + (1 - D_u).B_2)X + (D_u.C_1 + (1 - D_u).C_2] C \tag{3}$$

The steady-state of system has $X = \begin{bmatrix} I_{L_1} I_{L_2} & V_{C_1} V_{C_2} & I_{lo} \end{bmatrix}^T$ and $C = V_{in}$. Solving Eq. (3), the steady-state values of the capacitor voltages on C_1, C_2 and the inductor current through L_1, L_2 can be calculated as:

$$\begin{cases} V_{C_1} = \left(\frac{D'_u}{D'_u - D_u}\right).V_{in} = \left(\frac{1-D_u}{1-2D_u}\right).V_{in} \\ V_{C_2} = \left(\frac{D_u}{1-2D_u}\right).V_{in} \\ I_{L_1} = I_{L_2} = \left(\frac{D'_u}{D'_u - D_u}\right)^2 . \frac{V_{in}}{R_l} = \left(\frac{1-D_u}{1-2D_u}\right)^2 . \frac{V_{in}}{R_{lo}} \\ I_{lo} = \left(\frac{D'_u}{D'_u - D_u}\right) . \frac{V_{in}}{R_{lo}} = \left(\frac{1-D_u}{1-2D_u}\right) . \frac{V_{in}}{R_{lo}} \end{cases} \tag{4}$$

In NST, the relationship between DC-link voltage and input voltage is:

$$V_{dc} = V_{C_1} + V_{C_2} = \left(\frac{1}{1-2D_u}\right).V_{in} \tag{5}$$

From Eq. (4) and (5) the equation can be obtained as

$$\begin{cases} \frac{V_{C_1}}{V_{dc}} = 1 - D_u \\ \frac{V_{C_2}}{V_{dc}} = D_u \end{cases} \tag{6}$$

Refer in [12], the small signal state space equation can be written as

$$\begin{gathered} A.\dot{\hat{x}} = \left[D_u B_1 + (1-D_u) B_2\right].\hat{x} + \left[D_u C_1 + (1-D_u).C_2\right].\hat{c} \\ \left[(B_1 - B_2).X + (C_1 - C_2) C\right].\hat{c}\,(t) \end{gathered} \tag{7}$$

Based on equation of (7) and refer Eq. (12) to (15) in paper [12]. Transfer function of the capacitor voltage on C_1 with the shoot-through duty D_u is calculated as:

$$G_{v2d}(s) = \frac{\begin{gathered}\left(I_{lo} - I_{L_1} - I_{L_2}\right).L_{lo}.L.s^2 + \\ \left[L_{lo}.V_{in} + (1-D_u).L.\left(V_{C_1} + V_{C_2}\right) + R_{lo}.L.(I_{lo} - I_{L_1} - I_{L_2}).s\right] + V_{in}.R_{lo}\end{gathered}}{\begin{gathered}L_{lo}.L.C.s^3 + R_{lo}.L.C.s^2 + \left[L_{lo}.(1-2.D_u)^2 + 2(1-D_u)^2.L\right]s \\ + (1-2.D_u)^2.R_{lo}\end{gathered}} \tag{8}$$

And then, transfer function of the inductor current through L_1 with DC input voltage is calculated as:

$$G_{v2in}(s) = \frac{\begin{gathered}(1-D_u).L_{lo}.L.C.s^3 + (1-D_u).R_{lo}LC.s^2 + \left\{\left[(1-D_u)^2 - (1-D_u).D_u\right].L_{lo} + (1-D_u)^2.L\right\}.s + \\ \left(L.C.s^2 + 1\right) \times \\ \left[(1-D_u)^2 - (1-D_u).D_u\right].R_{lo}\end{gathered}}{\begin{gathered}\left\{L_{lo}LC.s^3 + R_{lo}.L.C.s^2 + \left[L_{lo}.(1-2D_u)^2 + 2(1-D_u)^2.L\right].s + (1-2D_u)^2.R_{lo}\right\}\end{gathered}} \tag{9}$$

Transfer function of the inductor current L_1 with the shoot-through duty cycle is obtained as

$$G_{i2d}(s) = \frac{\left(V_{C_1} + V_{C_2} - R_{lo}.I_{lo}\right).C.s + (2.D_u - 1)\left(I_{lo} - I_{L_1} - I_{L_2}\right) + V_{in}.R_{lo}}{L.C.s^2 + R_{lo}.L.C.s^2 + \left[L_{lo}.(1-2.D_u)^2 + 2(1-D_u)^2.L\right].s + (1-2.D_u)^2.R_{lo}} \tag{10}$$

$$G_{inv}(s) = \frac{1}{T_{sf}s + 1} \tag{11}$$

Table 1. Nominal Parameters of BQ-ZSI.

Parameters ($Units$)	Symbols	Values
Load current (A)	I_l	0.8
Inductor current on $L_1(H)$	I_{L_1}	0.7
Inductor current on $L_2(H)$	I_{L_2}	0.7
Switching frequency (kHz)	f_{sf}	5
Input voltage (V)	V_{in}	40
Load inductor (H)	L_l	17
Load resistor (Ω)	R_l	2.7
Shoot-through duty	$D_u = 1 - D'_u$	0.45
The proportional gain of current controller	K_{pi}	0.44
The integral gain of current controller	K_{ii}	4.4
The proportional gain of current controller	K_{pv}	0.0176
The integral gain of current controller	K_{iv}	0.264
Inductors of the BQ-ZSI (H)	$L_1 = L_2 = L$	$0.6 * 10^{-4}$
Capacitors of the BQ-ZSI (F)	$C_1 = C_2 = C$	$47 * 10^{-5}$

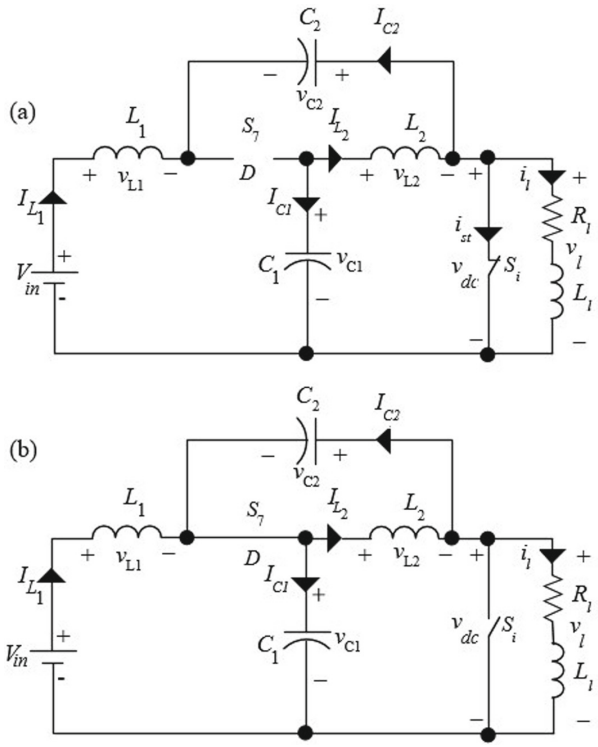

Fig. 3. Operation states of the BQ-ZSI.

3 Design of Controller for AC Side and DC Side

3.1 Adaptive Backstepping and Sliding Mode Controller (SA) for Speed Motor (AC Side)

In the functions of BQ-ZSI motor drive system, it is motor speed control (AC side control), which is designed to adapt to the torque motor and the tracking reference speed.

Adaptive Backstepping Controller is Presented in Fig. 1: The structure of adaptive backstepping controller for speed of PMSM, based on FOC and is shown in [6]. The position control of rotor according to tracking the reference position with the least error is the first priority of the controller. In the backstepping technique, it is transformed from the position tracking problem to the problem of tracking error. The position error is defined $e_\theta = \theta - \theta_r$, hence, its derivative is shown

$$\dot{e}_\theta = \dot{\theta} - \dot{\theta}_r = \omega - \dot{\theta}_r \tag{12}$$

The speed rotor reference is chosen as below

$$\omega_r = \dot{\theta}_r - k_1 e_\theta \tag{13}$$

where, $k_1 > 0$ and k_1 is a constant. Replacing equation of (13) into the (12), Eq. (12) is written as:

$$\dot{e_\theta} = -k_1 e_\theta \tag{14}$$

Based on Lyapunov theory, The function is chosen as

$$L_1 = \frac{1}{2} e_\theta^2 \tag{15}$$

And take the derivative Eq. (15) as

$$\dot{L}_1 = \dot{e}_\theta . e_\theta = -k_1 e_\theta^2 \leq 0 \tag{16}$$

The speed error is defined as $e_\omega = \omega - \omega_r$, speed error derivative $\dot{e}_\omega = \dot{\omega} - \dot{\omega}_r$ is and look at the Eq. (1), replacing $\dot{\omega}$ into its derivative which it is written as

$$\dot{e}_\omega = -\frac{B}{J}.\omega - \frac{T_L}{J} + \frac{1,5.n_p.\Psi_f}{J}.i_q - \dot{\omega}_r \tag{17}$$

The Lyapunov function can be chosen as $L_2 = \frac{1}{2} e_\omega^2$, take the derivative to get

$$\dot{L}_2 = e_\omega . \left(-\frac{B}{J}.\omega - \frac{T_L}{J} + \frac{1.5 n_p \Psi_f}{J} i_q - \dot{\omega}_r \right) \tag{18}$$

In FOC scheme, assuming that the virtual control variables are i_d and i_q currents. In order to get $\dot{L}_2 \leq 0$, from (18), it should be written as

$$-k_2 e_\omega = -\frac{B}{J}.\omega - \frac{T_L}{J} + \frac{1.5 n_p \Psi_f}{J} i_q - \dot{\omega}_r \tag{19}$$

where, k_2 is a constant and $k_2 > 0$. Hence, the virtual control current variable on q-axis is chosen as

$$\overset{*}{i}_q = \frac{J}{1.5 n_p \Psi_f}\left(-k_2.e_\omega + \frac{T_L}{J} + \frac{B}{J}.\omega + \dot{\omega}_r\right) \tag{20}$$

Due to the PMSM drive of the EV systems, the torque of the load often changes, and it has to be estimated so that it is possible to derive. Consequenstly, these i_d and i_q currents controllers is written as

$$\begin{cases} \overset{*}{i}_d = 0 \\ \overset{*}{i}_q = \frac{J}{1.5 n_p \Psi_f}\left(-k_2 e_\omega + \frac{\hat{T}_L}{J} + \frac{B}{J}.\omega + \dot{\omega}_r\right) \end{cases} \tag{21}$$

Substituting (21) into (18), it is derived

$$\dot{L}_2 = -k_2 e_\omega^2 \leq 0 \tag{22}$$

where, $k_2 > 0$, k_2 is a constant. Replacing (21) into (17), $\dot{e}_\omega$ is written as

$$\dot{e}_\omega = -k_2.e_\omega - \frac{\Delta T_L}{J} \tag{23}$$

Based on Lyapunov theory, the function of Lyapunov is designed to obtain a with the ability to attenuate the disturbance torque of the load. This Lyapunov fuction is chosen as belows equation:

$$L_3 = L_1 + L_2 + \frac{1}{2a}\left(T_L - \hat{T}_L\right)^2 \tag{24}$$

where a is the adaptive coefficient, $a > 0$. The Eq. (24) is derived as belows

$$\dot{L}_3 = -k_1 e_\theta^2 - k_2 e_\omega^2 + \Delta T_L\left(-\frac{e_\omega}{J} - \frac{\dot{\hat{T}}_L}{a}\right) \tag{25}$$

From (25), if $\dot{L}_3 \leq 0$ then $\Delta T_L\left(-\frac{e_\omega}{J} - \frac{\dot{\hat{T}}_L}{a}\right) = 0 \Longrightarrow -\frac{e_\omega}{J} - \frac{\dot{\hat{T}}_L}{a} = 0$
Therefore, the load torque is estimated as

$$\dot{\hat{T}}_L = -\frac{a.e_\omega}{J} \tag{26}$$

Sliding Mode Controller: The problem that is always exists in SMC is chattering problem. In order to reduce chattering, the surface of SMC and the reaching law have to be chosen a suitable. In this paper, the reaching law is chosen as the exponential reaching law (EL), as a result, the dynamic response of system moves quickly to the switching surface. This exponential reaching law is designed as

$$\dot{s} = -\left(1 - \frac{1}{e^{\lambda s} + 1}\right) - \delta s \tag{27}$$

The currents error on the $dq-$axis are defined as $\widetilde{i}_d = i_d - i_d^*, \widetilde{i}_q = i_q - i_q^*$. The Base on the currents error on $dq-$axis, the surfaces of SMC s_1 and s_2 are designed, respectively

$$s_1 = \gamma_1 \widetilde{i}_q = \gamma_1 \left(i_q - i_q^*\right) \tag{28}$$

$$s_2 = \gamma_2 \widetilde{i}_d = \gamma_2 \left(i_d - i_d^*\right) \tag{29}$$

where, γ_1 and γ_2 are constant, and $\gamma_1 > 0$, $\gamma_2 > 0$. The ELs are written as

$$\dot{s}_1 = -\left(1 - \frac{1}{e^{\lambda_1 s_1} + 1}\right) - \delta_1 s_1 \tag{30}$$

$$\dot{s}_2 = -\left(1 - \frac{1}{e^{\lambda_2 s_2} + 1}\right) - \delta_2 s_2 \tag{31}$$

where, λ_1, λ_2, δ_1, δ_2 are constant, $\gamma_1, \gamma_2 > 0$; and $\delta_1, \delta_2 > 0$.

From (1) and the derivative of (28), it is written as

$$\dot{s}_1 = \gamma_1 \left(\dot{i}_q - \dot{i}_q^*\right) = \gamma_1 \left(-n_p \omega i_d - \frac{R_s}{L_d} i_q - n_p \frac{\Psi_f}{L_q} \omega + \frac{1}{L_q} u_q - \dot{i}_q^*\right) \tag{32}$$

Based on the derivative of (28) equal (30),

$$\dot{s}_1 = -\left(1 - \frac{1}{e^{\lambda_1 s_1} + 1}\right) - \delta_1 s_1 = \gamma_1 \left(\dot{i}_q - \dot{i}_q^*\right)$$

$$\Longleftrightarrow \dot{i}_q = \frac{-\left(1 - \frac{1}{e^{\lambda_1 s_1 + 1}}\right) - \delta_1 s_1}{\gamma_1} + \dot{i}_q^* \tag{33}$$

Similarly, the current on q-axis is also obtained

$$\dot{i}_d = \frac{-\left(1 - \frac{1}{e^{\lambda_2 s_2 + 1}}\right) - \delta_2 s_2}{\gamma_2} + \dot{i}_d^* \tag{34}$$

Replacing (33) into (1), the control input u_q is achieved

$$u_q = L_q \left(\frac{-\left(1 - \frac{1}{e^{\lambda_1 s_1 + 1}}\right) - \delta_1 s_1}{\gamma_1} + \dot{i}_q^*\right) + n_p \omega i_d L_q + R_s i_q + n_p \Psi_f \omega \tag{35}$$

And the control input u_d is achieved as

$$u_d = L_d \left(\frac{-\left(1 - \frac{1}{e^{\lambda_2 s_2 + 1}}\right) - \delta_2 s_2}{\gamma_2} + \dot{i}_d^*\right) - \frac{R_s}{L_d} i_d - n_p \omega i_q \tag{36}$$

System Stability Analysis: Lyapunov function is defined (1) below

$$L = \frac{1}{2}s^T Is + \frac{1}{2}e_\theta^2 + \frac{1}{2}e_\omega^2 + \frac{1}{2a}\left(T_L - \hat{T}_L\right)^2 \tag{37}$$

The derivative of (37), it is obtained

$$\dot{L} = -\left(1 - \frac{1}{e^{\lambda_1 s_1}+1}\right)s_1 - \delta_1 s_1^2 - \left(1 - \frac{1}{e^{\lambda_2 s_2}+1}\right)s_2 - \delta_2 s_2^2 - k_2 e_\theta^2 - k_1 e_\omega^2 \tag{38}$$

with $\left(1 - \frac{1}{e^{\lambda_i s_i}+1}\right)s_i \geq 0$, if the system is a steady-state, then there are $e_\theta = e_\omega = 0$, $s_1 = s_2 = 0, \dot{L} = 0$. Therefore, $L \dot{\leq} 0$. Due to L is positive definite (38), and the PMSM drives system is a stable base on Lyapunov theory.

3.2 Design Controller for the DCV (DC Side Controller Design)

In the PMSM drive system, it contains DC-link voltage (DCV) control (DC side). When the DC input battery pack voltage (DIV) and the load torque of electric vehicle will be change continously depends on time, then the DCV (V_{dc}) can be controlled to stabilize the system. Although the DIV changes but the DCV is still kept stable when the DCV controller supplying the inverter is not short-circuited and the PMSM drive system works well.

In the BQ-ZSI system, there are two phases call ST and NST, with the DCV of BQ-ZSI is a square waveform [13]. During the NST, the DCV equals peak value of DCV $\left(\hat{V}_{dc}\right)$ and it equals zero in ST. Hence, the DCV can not be controlled directly but it has to be controlled by regulating total of two capacitors voltages [14]. From (4) and (5)the peak of DCV equals the capacitor voltage C_1 plus the capacitor voltage C_2 in BQZSI, it is uesd as the signal feedback of DCV in drive motor system Fig. 2 on page 3. Therefore, in this paper, the DCV voltage is controlled by controlling the total voltage across the two capacitors of the BQZSI as shown in Fig. 4 on page 12.

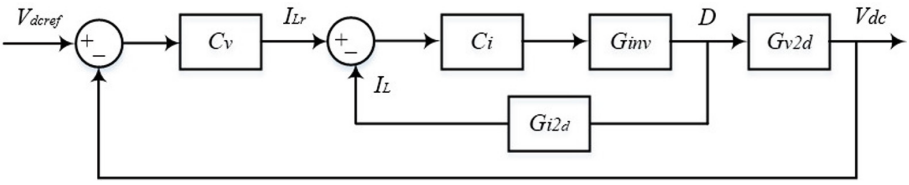

Fig. 4. Control block diagram of DC-link voltage loop.

In order to control the peak DCV voltage, transfer function of $G_{i2d}(s)$, $G_{inv}(s)$, $G_{v2d}(s)$are calculated base on (8), (9),(10), (11) where the parameters are used in 1. Using sisotool of Matlab, the first, PI controllers C_i is designed

with frequency-response approach so that I_{L_r} tracking I_L. After that, C_v is also designed with frequency-response as Fig. 5 on page 13. As result, these k_{p_i}, k_{i_i} of C_i and k_{p_v}, $k_{i_v}$of C_v are identified and updated into the system PMSM and simulated on Matlab software.

$$\begin{cases} C_i(s) = K_{p_i} + \frac{K_{i_i}}{s} \\ C_v(s) = K_{p_v} + \frac{K_{i_v}}{s} \end{cases} \tag{39}$$

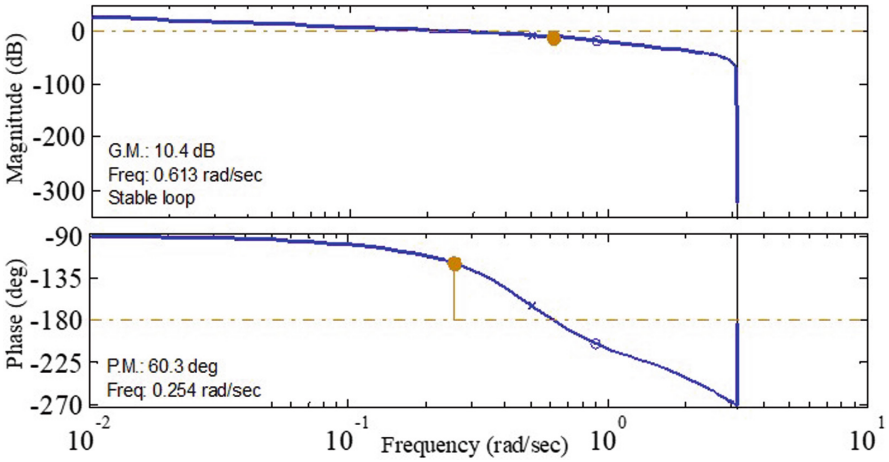

Fig. 5. Bode after designing PI controller for DCV.

4 Simulation

4.1 Simulation Result of PMSM

This simulation shows the motor speed response tracking reference motor speed under variations of the load torque and the DIV when applying backstepping control (SA) strategy with the parameters as in Table 2 [15].

Figure 6 page 14 presents the electromagnetic torque (T_e) which it tracks to the load torque (T_L). The SA strategy have a less ripple of the electromagnetic torque in comparision with the PI method. It also shows that the torque of load is continuous change at times t = 2 s, 4 s, the speed response of PMSM SA (red-line) are presented in Fig. 7 page 14 is able to achieve a better result than the motor speed response of PI controller (blue-line). In the simulation, the PMSM is started in unload operating mode, it shows that the speed of the PMSM is able to track the reference speed in a quickly manner.

At times t = 2 s, the nominal load torque suddenly increases from zero to 1.27 N.m as given in Fig. 6 on page 14, the speed response strategies as: SA

Table 2. Nominal Parameters of PMSM drives.

Parameters (*Units*)	Symbols	Values
Rated Power (W)	P_n	400
Rated Voltage (V)	U_n	200
Rated Speed (rpm)	c	3000
Rate Torque ($N.m$)	T_L	1.27
Permanent Magnet Flux (Wb)	Ψ_f	0.0615
Nominal Stator Resistance (Ω)	R_s	2.7
Nominal Stator Inductance (mH)	L_d, L_q	8.5
Moment of Inertia ($kg.m^2$)	J	$31.69 \times 10 - 6$
Viscous Friction Coefficient ($N.m.srad$)	B	$52.79 \times 10 - 6$
Pole Pair ($pair$)	n_p	4
The coefficient of adaptive backstepping	K_1	0.5
The coefficient of adaptive backstepping	K_2	40
The adaptive gain	a	0.001
The coefficient of SMC	γ_1	50
The coefficient of SMC	γ_2	50
The coefficient of SMC	λ_1	5
The coefficient of SMC	λ_2	5
The coefficient of SMC	δ_1	3000
The coefficient of SMC	δ_2	2000

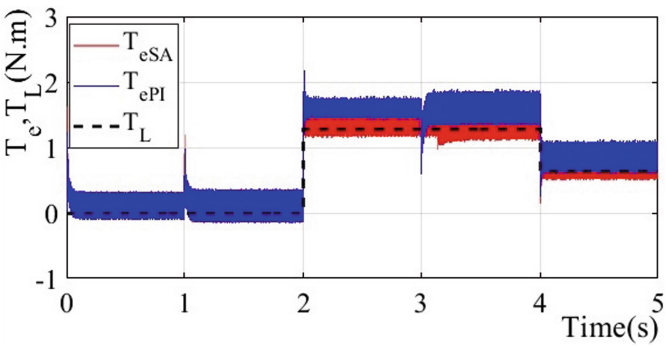

Fig. 6. Electromagnetic torque T_e and load torque T_L with PI, SA.

and PI that drops to 693 rmp and 638 rpm then are corrected back to speed reference value (≈700 rmp) after 0.2 s. Results showed that the SA has the lower than speed reduction compared to the PI controller and tracking error of the SA is also lower than the PI controller as Fig. 8 on page 15. Similar analysis, at times t = 4 s, the nominal load torque suddenly decreases from 1.27 to 1.27/2 N.m, as

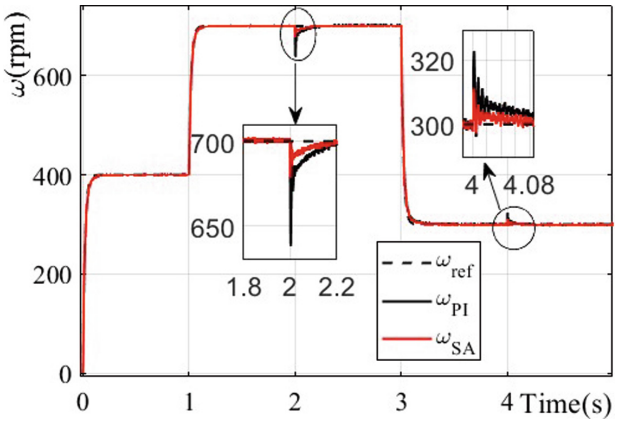

Fig. 7. Speed response with PI, SA.

given in Fig. 6 on page 14, the motor speed response with the different strategies as: SA and PI that rises up to 302 rmp, 311 rmp and 323 rpm then it comes back to speed reference value (≈300 rmp) after 4.1 s. Results also shows that the SA has the speed rise of the motor lower than the speed rise of the motor under PI controller as Fig. 8 on page 15.

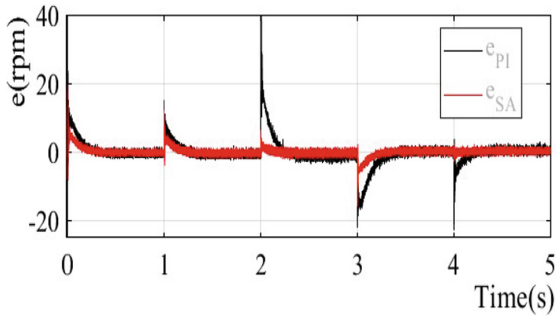

Fig. 8. Tracking errors using PI and SA controllers.

In the period, from t = 0 s to t = 1 s, the normal load torque is 0 N.m, the control voltage on $d-$axis, $u_d \approx 0$, i_d tracking zeros as shown in Fig. 9 on page 16. The control voltage on $q-$axis $(0 < u_q < 1)$ also changes to variation of the load torque and the motor speed in the PMSM drive system. Simulation results show that under normal operating modes as: the load torque and speed control variation, using the SA method gives smaller tracking error as compared to the PI controller Fig. 9 on page 16.

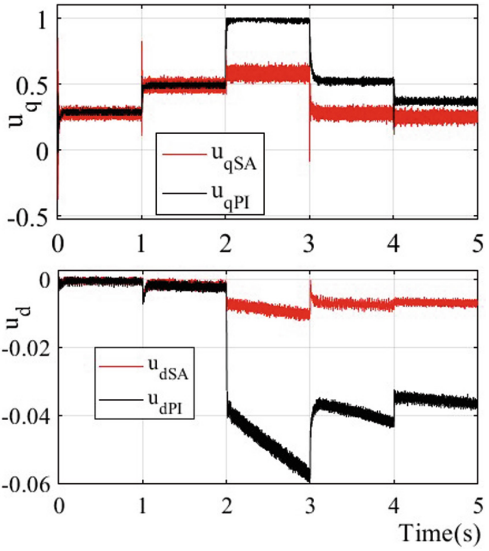

Fig. 9. The voltage control u_d, u_q with SA, PI controllers.

4.2 Simulation Result of BQ-ZSI

The DC-input voltage DIV (V_{in}) can be used for fuel cells or batteries. These sources are used as the supply voltage source for the BQ-ZSI and the PMSM applications for electric vehicles. Therefore, the purpose of DCV control is: to boost the DCV and keep it stable when the V_{in}, load torque and speed motor changes, to avoid overmodulation in the BQ-ZSI, thereby reducing harmonic of voltage and current, which ultimately improve the system performance.

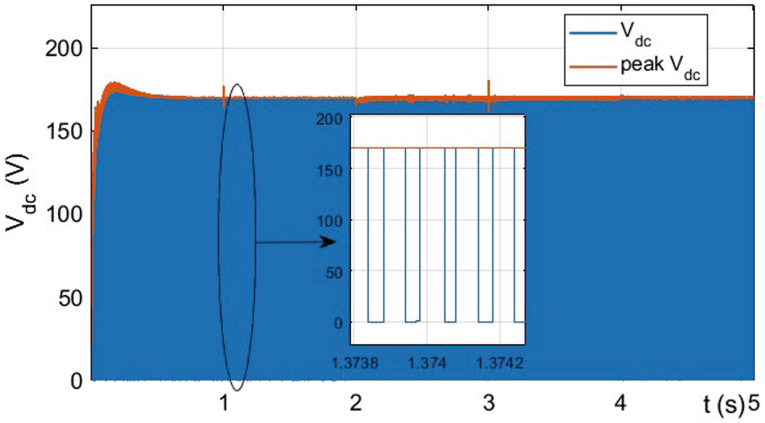

Fig. 10. a) The DC-link voltage V_{dc}. (Color figure online)

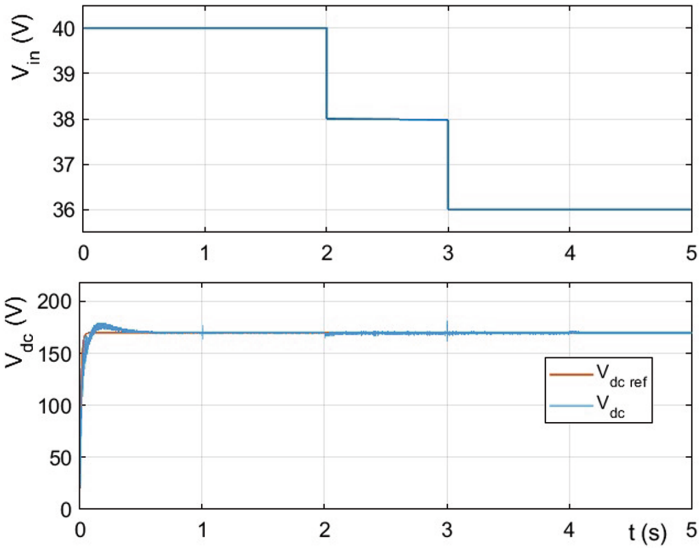

Fig. 11. a) V_{in} decreases by 5% after 1 s and continuously decreases by 5% after 2 s b) The response of the peakV_{dc} tracking V_{dcref} when the V_{in} and load torque change. (Color figure online)

Because the DCV is a square waveform is shown Fig. 10 on page 16, the DCV can not be controlled directly It must be controlled by regulating two capacitors voltages. Zoon "+" this waveform in Fig. 10 on page 16, from 1.3738 s to 1.3742, the DCV (blue line) is square waveform and the peak DCV equals total capacitor voltage on C_1 and C_2 of BQ-ZSI. That result is correct to Eq. (5).

From t = 0 s to t = 2 s, V_{in} has a value (40 V), at t = 2 s to 3 s, the V_{in} suddenly drops 5% (38 V). Continuously at t = 3 s to 5 s, the V_{in} also decreases by 5% (36 V) as shown in Fig. 11 on page 17 a). The DCV's required voltage is 170V as shown in Fig. 11 on page 17b) (red line), the BQ-ZSI unit is the booster, the voltage is raised from 40 V to 17 0V and stabilized at 170 V as shown Fig. 11 on page 17b) (blue line). If the input voltage changes, the DCV voltage remains stable at 170 V by the DCV controller. With this controller, the DCV track to the reference very well under the input voltage changes. And, this voltage is raised more than four times and is kept stable with variation of the input voltage, the speed motor and the load torque of the PMSM drive system.

5 Conclusion

In summary, this paper presents a comparison and evaluations of the different control strategies such as SA and PI for the speed control of PMSM. The SA enhances control quality of PMSM drive system, by compensating for the errors of the PI motor speed controller. Under normal operating conditions as

load torque, speed control and input voltage variation, applying the SA tracking method resulted in smaller errors compared to PI controllers. Besides, this study proposes a control method to stabilize the voltage of DCV in BQ-ZSI by controlling total two capacitor voltages in BQ-ZSI which yields an improvement to the system performance. These results have been verified carefully in simulation on the Matlab software.

Acknowledgment. The authors would like to thank the Vietnam Aviation Academy for Science and Technology Development for the support in 2022/2023.

References

1. Laoufi, C., Sadoune, Z., Abbou, A., Akherraz, M.: New model of electric traction drive based sliding mode controller in field oriented control of induction motor fed by multilevel inverter. Int. J. Power Electron. Drive Syst. (IJPEDS) **11**(1), 242–250 (2020)
2. Aghili, F.: Optimal feedback linearization control of interior PM synchronous motors subject to timevarying operation conditions minimizing power loss. IEEE Trans. Ind. Electron. **65**(7), 5414–5421 (2018)
3. Qu, L., Qiao, W., Qu, L.: An enhanced linear active disturbance rejection rotor position sensorless control for permanent magnet synchronous motors. IEEE Trans. Power Electron. **35**(6), 6175–6184 (2020)
4. Sun, Y., Preindl, M., Sirouspour, S., Emadi, A.: Unified wide-speed sensorless scheme using nonlinear optimization for IP-MSM drives. IEEE Trans. Power Electron. **32**(8), 6308–6322 (2017)
5. Massaq, Z., Abounada, A., Ramzi, M.: Robust non-linear control of a hybrid water pumping system based on in-duction motor. Int. J. Power Electron. Drive Syst. (IJPEDS) **11**(4), 1995–2006 (2020)
6. Tan, L.N., Pham, T.C.: Optimal tracking control for PMSM With partially unknown dynamics, saturation voltages, torque, and voltage disturbances. IEEE Trans. Ind. Electron. **69**(4), 3481–3491 (2022). https://doi.org/10.1109/TIE.2021.3075892
7. Bose, B.K.: Modern Power Electronics and AC Drives. Prentice-Hall, Upper Saddle River (2002)
8. Shen, A.W., Pham, C.T., Dzung, P.Q., Anh, N.B., Viet, L.H.: Using fuzzy logic self-tuning pi controller in z-source inverter for hybrid electric vehicles. In: 2012 World Conference on Science and Engineering, Hong Kong, China (2012)
9. Nguyen, T.N.A., Pham, D.C., Pham, C.T., Thanh, N.H.C.: D-axis stator current control methods applied to PMSG-based wind energy systems: a comparative study. WSEAS Trans. Syst. Control **14**, 239–239 (2019)
10. Wang, R., Jia, X., Dong, S., Zhang, Q.: PMSM driving system design for electric vehicle applications based on bi-directional quasi-Z-source inverter. In: 2018 13th IEEE Conference on Industrial Electronics and Applications (ICIEA) (2018)
11. Peng, F.Z.: Z-source inverter. IEEE Trans. Ind. Appl. **39**(2), 504–510 (2003)
12. Guo, F., Fu, L., Lin, C.H., et al.: Development of an 85-kW bidirectional quasi-Z-source inverter with DC-link feed-forward compensation for electric vehicle applications. IEEE Trans. Power Electron. **28**(12), 5477–5488 (2013)

13. Cong-Thanh, P., Anwen, S., Phan Quoc, D., Nguyen Bao, A., Nguyen Xuan, P.: A comparison of control methods for Z-source inverter. J. Energy Power Eng. **04**(04), 187–195 (2012)
14. Thanh, P.C., Wen, S.A.: A comparative study of control methods for induction motor and high performance Z-source inverter. TELKOMNIKA Ind. J. Electr. Eng. **11**(6), 2912–2925 (2013)
15. Tan, L.N., Cong, T.P., Cong, D.P.: Neural network observers and sensorless robust optimal control for partially unknown PMSM with disturbances and saturating voltages. IEEE Trans. Power Electron. **36**(10), 12045–2056 (2021)